A half-metallic semiDirac point generated by quantum confinement in TiO_2/VO_2 nanostructures

Victor Pardo[1,2,*] and Warren E. Pickett[1]

[1]*Department of Physics, University of California, Davis, CA 95616*

[2] *Departamento de Física Aplicada, Universidad de Santiago de Compostela, E-15782 Santiago de Compostela, Spain*

(Dated: December 16, 2008)

Study of layered oxide nanostructures has focused in large part on the polarity discontinuity that can give rise to unexpected electronic behaviour between insulating bulk oxides, including conductivity, magnetism, orbital order, even superconductivity. It is beginning to become clear that unanticipated factors can play an essential role, for example, strong repulsive interactions can drive two dimensional charge, spin, or orbital order, and polar distortions of cation-anion pairs can sustain strong screening across several unit cells, with each of these mechanisms serving to determine whether insulating or conducting behaviour results. The VO_2/TiO_2 interface involves no polar discontinuity but the multilayer structure seems to constrain the bulk VO_2 metal-insulator transition and accompanying lattice instability. The discontinuity at this interface is in the filling of the $3d$ **shell, which may lead to conductivity or magnetism depending on the response of the system to the change $d^1 \leftrightarrow d^0$ across the interface. By applying first principles density functional theory to these multilayers, we find that quantum confinement of the half metallic VO_2 slab within insulating TiO_2 produces an unexpected new electronic state, with a** ***semiDirac point*** **in VO_2 band structure that is a generalization of the much-studied Dirac point in graphene.**

VO_2 is a magnetic oxide that undergoes a metal-insulator transition[1] upon lowering the temperature through 340 K, accompanied of a symmetry-breaking structural transition from the high temperature metallic rutile phase[2]. The insulating state takes place via a dimerization of the V-V chains[3]. The origin of this metal-insulator transition is the focus of much recent theoretical activity and remains uncertain. It could be due to the formation of a Peierls state[4,5], or it could be driven by correlations[6,7], or more likely may have some mixed origin[8,9]. TiO_2 is isostructural (in one of its phases) and is a d^0 non-magnetic insulator that is very important industrially and is well understood.

The interface (IF) between a correlated insulator and a band insulator has been recognized as fertile ground for new behaviour,[10,11] and the $LaTiO_3/SrTiO_3$ (LTO/STO) IF involving the Mott insulator LTO has attracted much of the theoretical study to date.[12–14] For IFs between band insulators, $LaAlO_3/SrTiO_3$ (LAO/STO) has received a great deal of attention.[15–19] In both cases there is a polar discontinuity across the IF, and this aspect has been expected to dominate the resulting behaviour. In the LTO/STO case, first principles calculations including correlation effects indicate that the unbalanced formal charges at the IF leads to charge and orbital ordering in the ground state, and leave the system near a conducting/insulating crossover.[14,19]

The (001) VO_2/TiO_2 IF has been studied by photoemission spectroscopy (PES),[20] which found the IF is insulating when the VO_2 substrate is insulating. PES also has found[21] spectral weight transfer in VO_2/TiO_2 thin films indicating strong correlation effects even for conducting VO_2. Much of the focus on this nanostructure has been on tuning the VO_2 metal-insulator transition temperature[22], because of its potential technological applications. It has been found that a minimum thickness of 5 nm of VO_2 is needed to sustain a metal-insulator transition, for thinner VO_2 layers the transition no longer occurs[23] (the VO_2 layer remains conducting). The explanation is that the insulating state requires a collective structural dimerization along the rutile c-axis that is lost by confinement for thinner layers. Since the IF is not polar and the lattice mismatch is small (0.3 %), structural relaxation is not expected to be severe, a question that we have addressed (see Supplemental Information). Then any unusual behaviour of this multilayer (ML) will require different microscopic mechanisms than have been uncovered before.

We present a theoretical study of the electronic behaviour of the ML nanostructures $(TiO_2)_n/(VO_2)_m$, denoted (n/m), looking in particular at the evolution of the conduction and magnetic properties with VO_2 layer thickness. Since VO_2 is the component that is potentially conducting, we focus on thin VO_2 layers which will incorporate any consequences of quantum confinement. The properties are found to depend strongly on layer thickness and the effects of quantum confinement at small thicknesses give rise to a new electronic state for certain MLs.

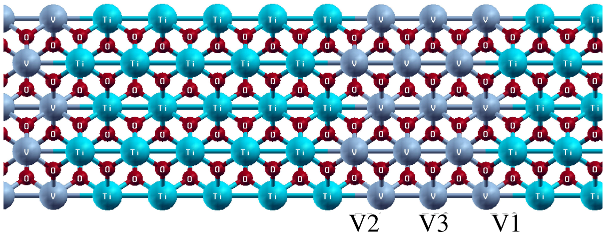

FIG. 1: Structure of the 3/5 VO_2/TiO_2 supercell corresponding to growth along the (001) axis, which is the metal chain direction of the rutile structure. V1, V2, V3 label the V ion sites beginning from the one nearest to TiO_2. (Due to a symmetry with respect to the centre of the VO_2 slab, the V layers are V1-V2-V3-V3-V2-V1.)

Starting from an average rutile structure of (n/m) MLs, we performed volume and c/a optimization and an internal relaxation of the atomic positions of all the atoms (based on total energy and forces minimization). The main modification is lattice strain along the c axis, interpolating between the slightly different c lattice constants. The absence of polarity accounts for the systematic relaxations; at polar IFs the ions move in response to electric fields caused by the local dipoles, but here no appreciable dipoles arise. We have studied several MLs, varying both TiO_2 and VO_2 layer thicknesses, following identical procedures. Our electronic structure calculations were performed within density functional theory[24] using the all-electron, full potential code WIEN2K[25] based on the augmented plane wave plus local orbital (APW+lo) basis set.[26] The exchange-correlation potential utilized to deal with possible strong correlation effects was the LSDA+U scheme[27,28] including an on-site U and J (on-site Coulomb repulsion and exchange strengths) for the Ti and V $3d$ states. We have used U=3.4 eV, J= 0.7 eV to deal properly with correlations in this multilayered structure, these values are comparable (slightly smaller) than what have been used for bulk VO_2.[9,29,30] (see Supplementary Information for more detail on this and other computational details, and the results of geometry relaxation). For these values of interaction strength, VO_2 remains metallic without V-V dimerization, in agreement with the corresponding observed conducting behaviour above 340 K, in rutile structure.

While we have studied a variety of n/m (001) MLs, we focus primarily on the (5/3) ML with 5 layers of TiO_2 (thickness of 1.5 nm) and 3 layers of VO_2 (0.9 nm thick). The structure, and the identification of the three distinct V sites, is shown in Fig. 1. In terms of distance from the TiO_2 layer, the V ions are labeled V1, V2, V3. We have retained the tetragonal symmetry of the rutile structure in the $x-y$ plane. By using the O $1s$ core levels across the IF as a reference energy, we determine the band alignment across the IF (see Supplementary Information for more discussion). From the largest nanostructures studied, we find that the Fermi level of VO_2 lies 1 eV above the bottom of the 3.0 eV gap of TiO_2.[31] This underlying band lineup is evident in the density of states (DOS) of the (5/3) ML in Fig. 2, where the half metallic Fermi level of this ferromagnetic (FM) ML lies 1.3 eV above the minority (TiO_2) band gap.

As anticipated, V $3d$ bands dominate the spectrum close to the Fermi level, and only three TiO_2 cells are required to give negligible k_z dispersion and thus confine the $3d$ states to a two dimensional system. FM alignment of the spins is preferred, and half metallicity results. From the enlarged projected density of states (DOS) in Fig. 2, it can be seen that although the spectral distribution is similar for V1, V2, and V3, the weight of the V1 ion (the one at the IF) vanishes just below the Fermi level (E_F). This curious DOS reflects a zero gap semiconductor involving V2 and V3 ion states.

The majority spin band structure along high symmetry directions shown in Fig. 2 clarifies an unexpected and quite anomalous electronic state. Two bands cross the Fermi level at a single point along the zone diagonal at the point k_{sD}=(0.37,0.37)π/a, but not along any other direction (the precise position of k_{sD} along the (1,1) direction depends on the value of U). Inspection throughout the zone confirms that this Fermi surface crossing is a single point (rather, four symmetry related points), as is the Dirac point in graphene.[32] This single point determines the Fermi energy, again as in graphene.[34] The crossing of the bands precisely at E_F is therefore not accidental, rather it is topologically determined: there are exactly six filled bands below this point, containing the majority spin electrons of each of the six V ions in the cell.

These two bands crossing E_F involve separately V2 and V3 ion $3d$ states, as is illustrated with the colour coded fatbands in Fig. 2. With no contribution from the IF ion V1, the dominance of V2 and V3 bands is identified as a *quantum confinement effect* rather than an IF phenomenon. In Fig. 3 we provide a surface plot display of these two band energies plotted in a small region in k-space centered on the band crossing point k_{sD}. As discussed in the Supplementary Information, this state results only after the ion positions are relaxed, and arises due to band reordering at k=0 that occur during the relaxation. The surface plot reveals yet another peculiarity: while the dispersion is linear along the (1,1) direction as is clear from the band plot, the dispersion is *quadratic* perpendicular to the diago-

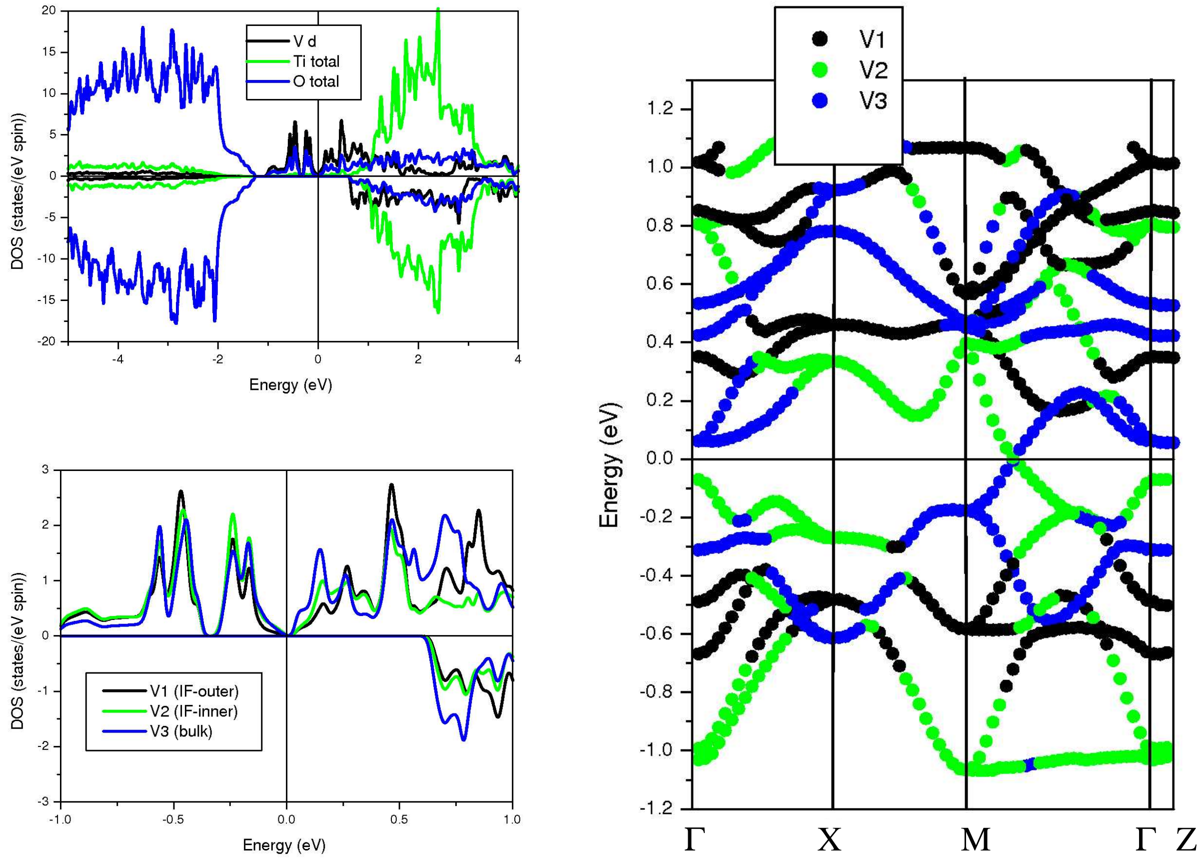

FIG. 2: Left upper panel: Total density of states in the 5/3 multilayer, indicating the location of the V and Ti bands. Left lower panel: Partial density of states of the three inequivalent V atoms in the structure. Most of the weight around the Fermi level comes from V3 and V2. The outer interfacial V1 ions' d^1 state is fully occupied by a bonding-antibonding pair of bands below the Fermi level. Right panel: Blow-up of the band structure around the Fermi level showing in different colours the biggest character of each band. Notice that the two bands crossing at the Fermi level have character from the two most inner V atoms.

nal; the gap opens due to the loss of symmetry of the two bands off the diagonal $k_x = k_y$, and does so quadratically. To differentiate this point from the graphene Dirac point, we refer to it as the (half metallic) semiDirac (sD) point. The corresponding mass tensor shows extreme anisotropy (zero to normal values), as does the velocity (1.5×10^7 cm/s to zero).[32] This very strongly anisotropic dispersion, between extremes (normal values, to zero) will give rise to peculiar transport and thermodynamic properties (to be discussed elsewhere).

The constant energy surfaces for both electrons and holes are plotted in the right panel of Fig. 3 for low energies in a small region around k_{sD}. The conduction band has a flatness that opens a path for a Fermi surface to develop as a ring around the M=(π, π) point at very low electron doping. The valence band shows iso-energetic contours with an elliptical shape, with the longer axis perpendicular to the zone diagonal.

In bulk VO_2 (V^{4+}: d^1 cations) the distortion from cubic symmetry of the VO_6 octahedron introduces a crystal field (actually, ligand field) that lifts the degeneracy of the t_{2g} orbitals, splitting them into a $d_\parallel$ singlet and two $d_\perp$ orbitals (using Goodenough's notation[4]). The orbital ordering that arises in this 5/3 ML is illustrated by the spin density isosurfaces in Fig. 4, where the orientation of the occupied orbital (orbital ordering) of the V cations is clear. The V ions (V1 and V2) that terminate a V-V-V chain have an occupied $d_\parallel$ orbital, whereas the chain-center V3 ion has an occupied orbital of $d_\perp \propto d_{xz}+id_{yz}$ character. This orbital ordering is dependent on the magnetic ordering; when the spins along

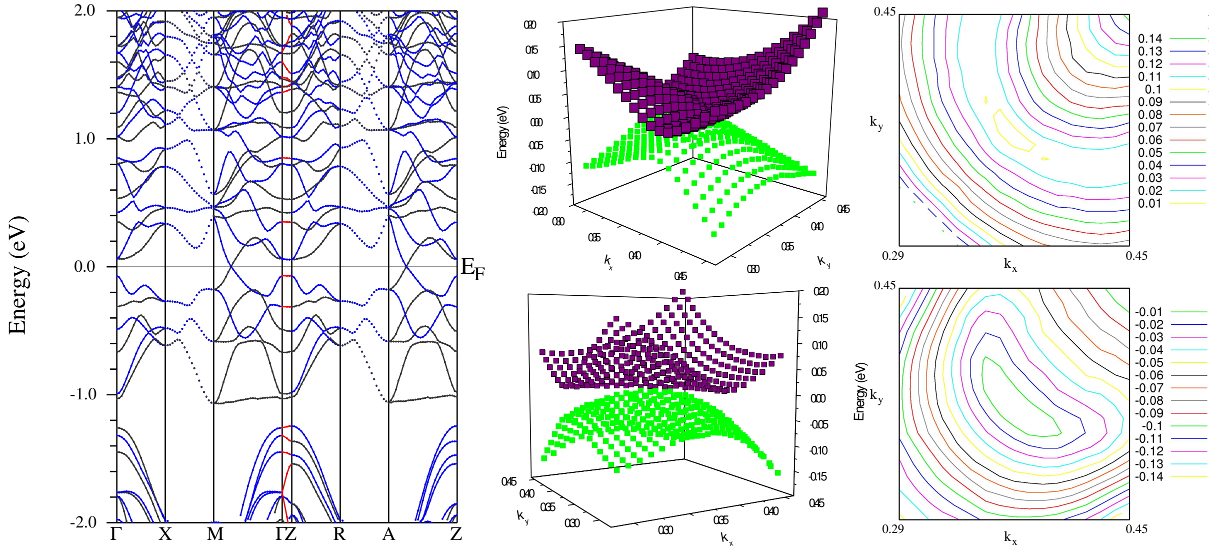

FIG. 3: Left panel: Majority spin band structure in a tetragonal Brillouin zone. Bands related by symmetry are plotted as same-colour lines; only bands of different symmetries are allowed to cross. Note the semiDirac point along the (110) direction where bands cross precisely at the Fermi level. Middle panel: Two different views of the same 'surface' plot of the two bands that cross the Fermi level, centered around the semiDirac point. The valence and conduction bands cross at a single point. The linear dispersion can be seen in the upper plot (upper left and lower right); the quadratic dispersion is clear in the lower panel, where the flatness of the conduction band is also clear. Right panel: contour plots at constant energy (in eV, relative to the Fermi level) of the valence band (below), and the flat conduction band (above) that leads to large M-centered Fermi surfaces.

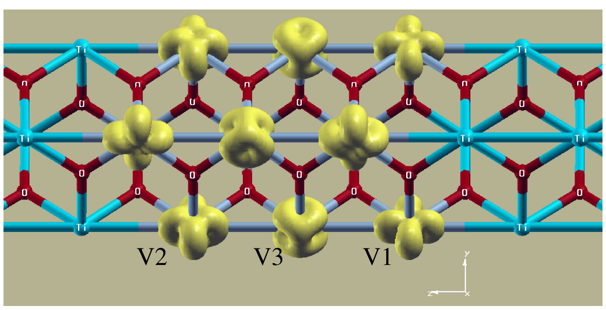

FIG. 4: Spin density plot, isosurface at 0.15 e/Å^3. The particular orbital ordering in a spin-aligned configuration is shown. V1 and V2 have one electron in a $d_\perp$ and V3 is in a $d_\parallel$ orbital.

the c direction are antialigned (↑↓↑) the $d_\parallel$ becomes occupied in all sites. The FM state is energetically favored over this ferrimagnetic state. For a discussion on energetics of the various possible magnetic states, see Supplementary Information. The corresponding bands hybridize little, as emphasized by Eyert,[33] and due to the planar symmetry the hybridization vanishes along the (1,1) directions, allowing the formation of the semiDirac point.

Influence of VO_2 slab thickness. A metal-insulator transition is observed[23] for VO_2 thicknesses above 5 nm (approximately 15 layers), but experimental information on crystalline samples with smaller thickness is lacking. Our calculations show that the system has an insulating ground state for two layers of VO_2. However, for thicknesses of approximately one nm (3 layers), the material is in the intermediate zero-gap semiDirac state described above, on the brink of metallicity. Thicker VO_2 layers (four or more) become half metallic, a property that is much sought in oxide nanostructures because of its potentially enormous technological applications in spintronic devices.

Influence of magnetic alignment. We have studied antialignment of the moments (ferrimagnetism) along the (001) V-V chains. Such AF coupling is energetically unfavourable in almost all cases. Interestingly, such antialignment changes the orbital ordering: in the 5/3 multilayer (the semiDirac point system when FM), flipping the spin of the intermediate V ion (V2) results in all V ions having an occupied $d_\parallel$ orbital, because the σ-bond along the z-axis between neighboring $d_\parallel$ orbitals favours AF coupling.

Role of V-Ti exchange disorder. States that are very sensitive to disorder are less likely to have importance in applications, since thin film growth does not result in perfectly ordered materials. We have studied the effect of V/Ti exchange near the IF on the electronic properties. We find that the most unexpected feature, *i.e.* the development of a half metallic semiDirac point for three VO_2 layers, is robust with respect to two types of ion exchange that do not change the electron count, *i.e.* no doping. The first type was the interchange of V1 with Ti across the IF, which is a typical defect in growth. If we label the Ti sites across the multilayer as Ti1/Ti2/Ti3/Ti4/Ti5/Ti5/Ti4/Ti3/Ti2/Ti1, this first type of disorder corresponds to the interchange of V1 and Ti1, corresponding to a non-abrupt IF. The second type is to interchange V1 with Ti2, which are neighbours along the cation chain. In both cases a semiDirac point persists in spite of changes of the band structure.

We have studied the robustness of this unusual property in the band structure for the 3-layer VO_2 system with respect to the thickness of the TiO_2 layer. Reduction of TiO_2 thickness to just three layers changes slightly the position of the crossing point in the Brillouin zone, but still gives negligible dispersion along the z-axis, *i.e.* the behavior is still two dimensional. The semiDirac point is also robust with respect to the strength of correlation effects: the semiDirac point varies along the diagonal from (0.3,0.3,k_z) to (0.4,0.4,k_z) depending on both the choice of U (for reasonable values, above 2 eV) and TiO_2 thickness, but it persists along the diagonal symmetry line in the Brillouin zone.

The finding that quantum confinement in oxide multilayers can produce a semiDirac point as the crossover between insulating and conducting behaviour introduces a novel feature in the physics of oxide heterostructures: a polar discontinuity is not required to produce unexpected and unprecedented electronic states in these systems. The conduction behaviour, and the changes with doping, for systems with a semiDirac point will be addressed in following papers. In addition, oxide nanostructures are mechanically more robust than graphene, and patterning of such multilayers is readily accessible.

This project was supported by DOE grant DE-FG02-04ER46111 and through interactions with the Predictive Capability for Strongly Correlated Systems team of the Computational Materials Science Network and a collaboration supported by a Bavaria-California Technology grant. V.P. acknowledges financial support from Xunta de Galicia (Human Resources Program).

I. SUPPLEMENTARY INFORMATION

A. Computational details

Electronic structure calculations were performed within density functional theory[24] using WIEN2K,[25] which utilizes an augmented plane wave plus local orbitals (APW+lo)[26] method to solve the Kohn-Sham equations. This method uses an all-electron, full-potential scheme that makes no shape approximation to the potential or the electron density. The exchange-correlation potential utilized to deal with possible strong correlation effects was the LSDA+U scheme[27,28] including an on-site U and J (the on-site Hund's rule coupling constant) for the Ti and V d states. We have used a value of U and J so that rutile VO_2 is metallic. For values of U-J bigger than 3.5 eV, VO_2 rutile becomes incorrectly insulating, indicating that correlations are being overestimated. Hence, we have used U= 3.4 eV, J= 0.7 eV to deal properly with correlations in this multilayered structure. Muffin-tin radii chosen were 1.85 a.u. for Ti and V, and 1.64 a.u. for O. A k-mesh $8 \times 8 \times 1$, and $R_{mt}K_{max}$= 6 were utilized. All the calculations were converged with respect to all the parameters used, to the precision necessary to support our calculations, specially forces on the structure minimization, which was performed using the LSDA+U method. The orbital occupancies and the local symmetry around the V atoms do not vary significantly by varying U and J within the limits 2.0 eV $\leq$ U-J $\leq$ 3.5 eV, showing the robustness of the results presented.

B. Band alignments

Referencing to the O 1s core levels is an efficient way to determine the band line-up across the interface. The left panel of Fig. 5 shows that the O 1s core level position converges (to the bulk value) within the TiO_2 layer, but perhaps not quite in the thinner VO_2 layer. Still, this amounts to only a minor correction of the band alignments. The resulting band line-up is shown in the right panel of Fig. 5: the Fermi level of VO_2 lies 1.0 eV above the bottom of the 3.0 eV gap of TiO_2.

C. Structural relaxation

The structural relaxation we have carried out includes a volume, c/a and atomic position optimization corresponding to a periodic multilayer film. Relaxation was performed using the LSDA+U method, as explained above. It leads to the following distances for the 5/3 multilayer. The interior layers of

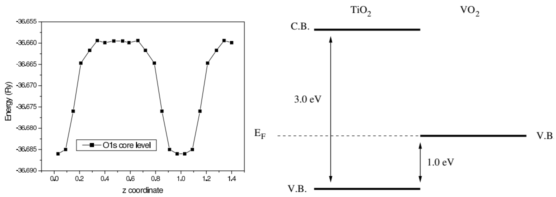

FIG. 5: Left panel: O 1s core level energies, plotted versus the z position across the multilayer. Right panel: band alignments across the interface, showing that the Fermi level falls 1.0 eV above the bottom of the 3.0 eV TiO_2 band gap.

TiO_2 are separated by 2.93 Å, 1% less than the experimental bulk value and typical of DFT accuracy. However, VO_2 layer separations are different than in bulk, showing signs of quantum confinement within insulating TiO_2. The manner in which the distance between cations varies along the z-direction is shown in Fig. 6. The octahedral oxygen cages around the V atoms are changed very little compared to bulk. The main structure relaxation is strain along the c-axis, leading to an average c-lattice parameter 2.87 Å, and a-lattice parameter of 2.78 Å (experimental bulk values are TiO_2: 4.59 / 2.96; VO_2: 4.55 / 2.86)[23].

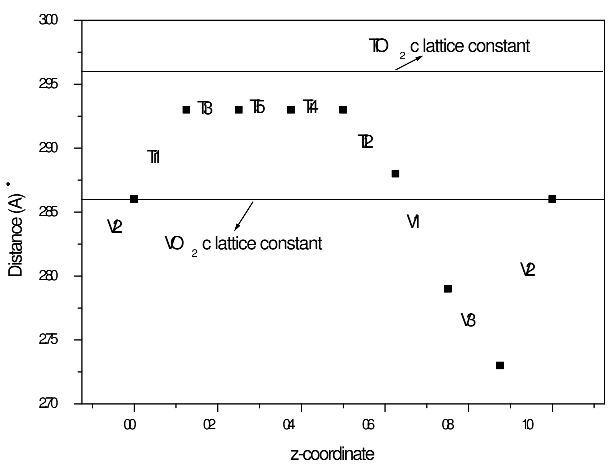

FIG. 6: Cation-cation distance across the multilayer along the c-direction. The bulk experimental lattice parameters of TiO_2 and VO_2 are shown on the graph for the sake of comparison.

The structural relaxation affects the electronic structure. The band structure of the unrelaxed structure, which is a weighted average of the rutile structures of VO_2 and TiO_2, with the oxygen ions in the same Wyckoff site 4f (0.3,0.3,0.3) position as in the bulk materials, and with a= 4.59 Å (bulk value for TiO_2). With this structure (which is artificially strained), the two bands close to the Fermi level do not cross. During the structural relaxation bands reorder at k=0, leading to the band crossing and the semiDirac point. The details of the electronic structure are not strongly dependent on the oxygen cages; it is the cation neighbour positions that are the determining factor. The occurrence of the semiDirac point is independent of whether structural relaxation is done including on-site Coulomb repulsion U or not, and also is independent of whether a full volume and c/a optimization is performed or not.

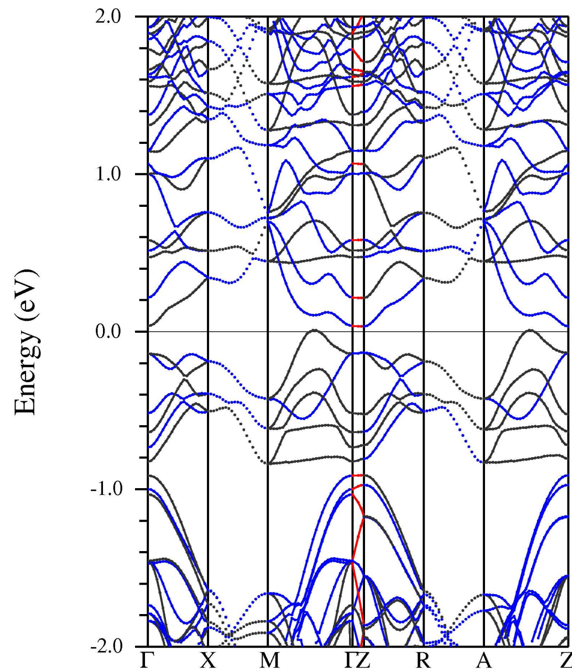

FIG. 7: Band structure of the 5/3 multilayer in the unrelaxed rutile structure. No band crossing occurs before strain along the c-axis is allowed. The material is a small-gap insulator in this case. This shows that the semiDirac point is brought about by lattice strain.

D. Magnetic in-chain couplings

We have studied different magnetic alignments along the c-axis. Both ferromagnetic (FM) and "antiferromagnetic" (AF) V-V spin alignments have been studied. In bulk VO_2, the chain dimerization is suggested by some to give rise to spin-singlet VO_2 dimers, which would be favoured by AF coupling. Such dimerization in a finite chain would be disfavoured by an odd number of spins in a chain. The quantum effect of singlet formation is however not included in our density functional calculations. For 2 VO_2 layers in the 5/2 multilayer, AF coupling is more stable by 9 meV/V and the slab is insulating, while for 4 VO_2 layers (the 5/4 multilayer) FM alignment is more stable by 27 meV/V and the slab is half metallic. As mentioned earlier, FM alignment giving half metallicity is favored for the 5/3 multilayer with the semiDirac point.

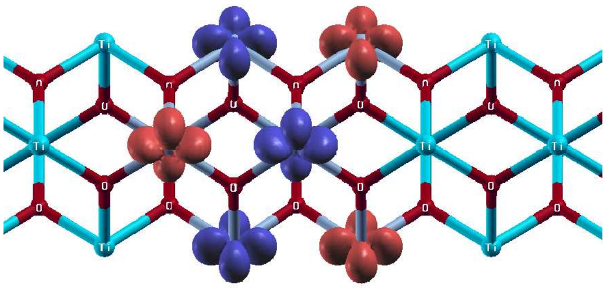

FIG. 8: Spin density isosurface plot at 0.15 e/Å^3 showing the orbital configuration in the 5/2 multilayer. Observe the σ-bond along the c-axis that takes place when neighbour V atoms have the same $d_{\parallel}$ orbital occupied.

Figure 8 shows the spin density isosurface plots for the AF case of the 5/2 multilayer. The σ-bond along the rutile c-axis can be seen, favouring the spin antialignment. The AF in-chain coupling favours the occupation of the $d_{\parallel}$ orbital, reflecting the connection between magnetic and orbital ordering. Both types of order influence the conducting versus insulating behaviour.

E. Energetics of the disordered cases

Figure 9 shows the two V↔Ti exchanged structures we have studied, which are the simplest cases of non-ideal growth that can be studied without doping. The top panel shows a 'non-abrupt' interface between TiO_2 and VO_2, which corresponds to interchanging V1 with Ti1, the two ions at the IF. The lower panel shows the case V1↔Ti2, corresponding to exchange of V and Ti along a cation chain. The energies involved in these "disordered" cases studied are fairly small: both of these structures are isoenergetic (within 0.3 meV/metal), and are about 15 meV/cation higher in energy than the perfect 5/3 multilayer.

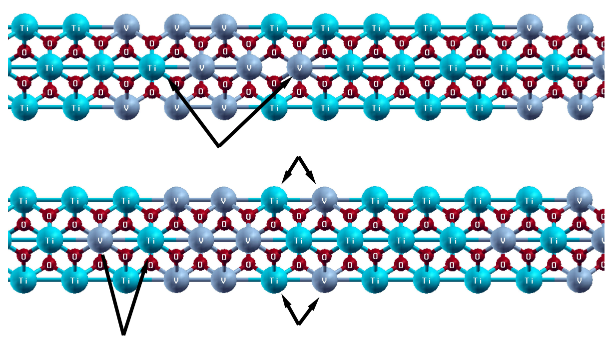

FIG. 9: Disordered interfaces we have studied. Above a non-abrupt type of IF formed by interchanging V1 and Ti1. Below, an IF formed by interchanging V1 and Ti2, that leads to a semilayer of VO_2 introduced in the TiO_2 layer.

* Electronic address: victor.pardo@usc.es

[1] Morin, F. J. Oxides Which Show a Metal-to-Insulator Transition at the Neel Temperature. *Phys. Rev. Lett.* **3**, 34 (1959).

[2] McWhan, D. B., Marezio, M., Remeika, J. P., and Dernier, P. D. X-ray diffraction study of metallic VO_2. *Phys. Rev. B* **10**, 490 (1974).

[3] Marezio, M., McWhan, D. B., Remeika, J. P., and Dernier, P. D. Structural Aspects of the Metal-Insulator Transitions in Cr-Doped VO_2. *Phys. Rev. B* **5**, 2541 (1972).

[4] Goodenough, J. B. 2 components of crystallographic transition in VO_2. *J. Solid State Chem.* **3**, 490 (1971).

[5] Wentzcovitch, R. M., Chulz, W. W., and Allen, P. B. VO_2 Peierls or Mott-Hubbard? A view from band theory. *Phys. Rev. Lett.* **72**, 3389 (1994).

[6] Zylbersztejn, A. and Mott, N. F. Metal-insulator transition in vanadium dioxide. *Phys. Rev. B* **11**, 4383 (1975).

[7] Laad, M. S., Craco, L., and Mueller-Hartmann, E. VO_2: A two-fluid incoherent metal?. *Europhys. Lett.* **69**, 984 (2005).

[8] Paquet, D. and Leroux-Hugon, P. Electron correlations and electron-lattice interactions in the metal-insulator, ferroelastic transition in VO_2: A thermodynamical study. *Phys. Rev. B* **22**, 5284 (1980).

[9] Biermann, S., Poteryaev, A., Lichtenstein, A. I., and Georges, A. Dynamical Singlets and Correlation-Assisted Peierls Transition in VO_2. *Phys. Rev. Lett.* **94**, 026404 (2005).

[10] Ohtomo, A., Muller, D. A., Grazul, J. L., and Hwang, H. Y. Artificial charge-modulationin atomic-scale perovskite titanate superlattices. *Nature* **419**, 378 (2002).

[11] Ohtomo, A. and Hwang, H. Y. A high-mobility electron gas at the $LaAlO_3/SrTiO_3$ heterointerface. *Nature* **427**, 423 (2004).

[12] Hamann, D. R., Muller, D. A., and Hwang, H. Y. *Phys. Rev. B* **73**, 195403 (2006).

[13] Okamoto, S., Millis, A. J., and Spaldin, N. A. Lattice relaxation in oxide heterostructures: $LaTiO_3/SrTiO_3$ superlattices. *Phys. Rev. Lett.* **97**, 056802 (2006).

[14] Pentcheva, R. and Pickett, W. E. Correlation-driven charge order at the interface between a Mott insulator

and a band insulator. *Phys. Rev. Lett.* **99**, 016802 (2007).

[15] Pentcheva, R. and Pickett, W. E. Ionic relaxation contribution to the electronic reconstruction at the n-type $LaAlO_3/SrTiO_3$ interface. *Phys. Rev. B* **78**, 205106 (2008).

[16] Siemons, W., Koster, G., Yamamoto, H., Harrison, W. A., Lucovsky, G., Geballe, T. H., Blank, D. H. A., and Beasley, M. R. Origin of charge density at $LaAlO_3$ on $SrTiO_3$ Heterointerfaces: Possibility of intrinsic doping. *Phys. Rev. Lett.* **98**, 196802 (2007).

[17] Willmott, P. R., Pauli, S. A., Herger, R., Schlepütz, C. M., Martoccia, D., Patterson, B. D., Delley, B., Clarke, R., Kumah, D., Cionca, C., and Yacoby, Y. Structural basis for the conducting interface between $LaAlO_3$ and $SrTiO_3$. *Phys. Rev. Lett.* **99**, 155502 (2007).

[18] Park, M. S., Rhim, S. H., and Freeman, A. J. Charge compensation and mixed valency in $LaAlO_3/SrTiO_3$ heterointerfaces studied by the FLAPW method. *Phys. Rev. B* **74**, 205416 (2006).

[19] Pentcheva, R. and Pickett, W. E. Charge localization or itineracy at $LaAlO_3/SrTiO_3$ interfaces: Hole polarons, oxygen vacancies, and mobile electrons. *Phys. Rev. B* **74**, 035112 (2006).

[20] Maekawa, K., Takizawa, M., Wadati, H., Yoshida, T., Fujimori, A., Kumigashira, H., Oshima, M., Muraoka, Y., Nagao, Y., and Hiroi, Z. Photoemission study of TiO_2/VO_2 interfaces. *Phys. Rev. B* **76**, 115121 (2007).

[21] Okazaki, K., Sugai, S., Muraoka, Y., and Hiroi, Z. Role of electron-electron and electron-phonon interaction effects in the optical conductivity of VO_2. *Phys. Rev. B* **73**, 165116 (2006).

[22] Muraoka, Y. and Hiroi, Z. Metal-insulator transition of VO_2 thin films grown on TiO_2 (001) and (110) substrates. *Appl. Phys. Lett.* **80**, 583 (2002).

[23] Nagashima, K., Yanagida, T., Tanaka, H., and Kawai, T. Interface effect on metal-insulator transition of strained vanadium dioxide ultrathin films. *J. Appl. Phys.* **101**, 026103 (2007).

[24] Hohenberg, P. and Kohn, W. Inhomogeneous Electron Gas. *Phys. Rev.* **136**, B864 (1964).

[25] Schwarz, K. and Blaha, P. Solid state calculations using WIEN2k. *Comp. Mat. Sci.* **28**, 259–273 (2003).

[26] Sjöstedt, E., Nördstrom, L., and Singh, D. J. An alternative way of linearizing the augmented plane-wave method. *Solid State Commun.* **114**, 15 (2000).

[27] Anisimov, V. I., Zaanen, J., and Andersen, O. K. Density functional theory for Mott insulators. *Phys. Rev. B* **44**, 943 (1991).

[28] Ylvisaker, E. R., Pickett, W. E., and Koepernik, K. Anisotropy and magnetism in the LSDA+U method. *Phys. Rev. B* , accepted (2008).

[29] Tomczak, J. M. and Biermann, S. Effective band structure of correlated materials: the case of VO_2. *J. Phys.: Condens. Matter* **19**, 365206 (2007).

[30] Haverkort, M. W., Hu, Z., Tanaka, A., Reichelt, W., Streltsov, S. V., Korotin, M. A., Anisimov, V. I., Hsieh, H. H., Lin, H. J., Chen, C. T., Khomskii, D. I., and Tjeng, L. H. Orbital-assisted metal-insulator transition in VO_2. *Phys. Rev. Lett.* **95**, 196404 (2005).

[31] Pascual, J., Camassel, J., and Mathieu, H. Fine structure in the intrinsic absorption edge of TiO_2. *Phys. Rev. B* **18**, 5606 (1978).

[32] Novoselov, K. S., Geim, A. K., Morozov, S. V., Jiang, D., Kastnelson, M. I., Grigorieva, I. V., Dubonos, S. V., and Firsov, A. A. Two-dimensional gas of massless Dirac fermions in graphene. *Nature* **438**, 197 (2005).

[33] Eyert, V. The metal-insulator transitions of VO_2: A band theoretical approach. *Ann. Phys. (Leipzig)* **11**, 650 (2002).

[34] Katsnelson, M. I. Graphene: carbon in two dimensions. *Materials Today* **10**, 20 (2007).